Quantifying volumetric scattering bias in ICESat-2 and Operation IceBridge altimetry over snow-covered surfaces

Fair Zachary[1], Flanner Mark[2], Neumann Thomas A[3], Vuyovich Carrie[3], Smith Benjamin E.[4], and Schneider Adam Michael[5]

[1]Goddard Space Flight Center
[2]University of Michigan-Ann Arbor
[3]NASA Goddard Space Flight Center
[4]Un. Washington
[5]University of California, Irvine

November 16, 2022

Abstract

The Ice, Cloud, and Land Elevation Satellite-2 (ICESat-2) mission has collected global surface elevation measurements for over three years. ICESat-2 carries the Advanced Topographic Laser Altimeter (ATLAS) instrument, which emits laser light at 532 nm, and ice and snow absorb weakly at this wavelength. Previous modeling studies found that melting snow could induce significant bias to altimetry signals, but there is no formal assessment on ICESat-2 acquisitions during the Northern Hemisphere melting season. In this work, we performed two case studies over the Greenland Ice Sheet to quantify volumetric scattering in ICESat-2 signals over snow. Elevation data from ICESat-2 was compared to Airborne Topographic Mapper (ATM) data to quantify bias. We used snow optical grain sizes derived from ATM and the Next Generation Airborne Visible/Infrared Imaging Spectrometer (AVIRIS-NG) to attribute altimetry bias to snowpack properties. For the first case study, the mean optical grain sizes were 340±65 µm (AVIRIS-NG) and 670±420 µm (ATM), which corresponded with a mean altimetry bias of 4.81±1.76 cm in ATM. We observed larger grain sizes for the second case study, with a mean grain size of 910±381 µm and biases of 6.42±1.77 cm (ICESat-2) and 9.82±0.97 cm (ATM). Although these altimetry biases are within the accuracy requirements of the ICESat-2 mission, we cannot rule out more significant errors over coarse-grained snow, particularly during the Northern Hemisphere melting season.

Quantifying volumetric scattering bias in ICESat-2 and Operation IceBridge altimetry over snow-covered surfaces

Zachary Fair[1], Mark Flanner[2], Tom Neumann[1], Carrie Vuyovich[1], Benjamin Smith[3], Adam Schneider[4]

[1]NASA Goddard Space Flight Center, Greenbelt, MD, USA
[2]Department of Climate and Space Sciences and Engineering, University of Michigan, Ann Arbor, MI, USA
[3]Applied Physics Laboratory, University of Washington, Seattle, WA, USA
[4]Department of Earth System Science, University of California, Irvine, CA, USA

Key Points:

- The effects of snow density and optical grain size on ICESat-2 and Operation IceBridge lidar signals were characterized.
- Both altimeters experienced centimeter-level bias that is linked to the optical grain size of snow over the Greenland Ice Sheet.
- A strong agreement between ICESat-2 and modeled bias suggests that retrieved ATL03 photons are sensitive to subsurface snow properties.

Corresponding author: Zachary Fair, `zachary.fair@nasa.gov`

Abstract

The Ice, Cloud, and Land Elevation Satellite-2 (ICESat-2) mission has collected global surface elevation measurements for over three years. ICESat-2 carries the Advanced Topographic Laser Altimeter (ATLAS) instrument, which emits laser light at 532 nm, and ice and snow absorb weakly at this wavelength. Previous modeling studies found that melting snow could induce significant bias to altimetry signals, but there is no formal assessment on ICESat-2 acquisitions during the Northern Hemisphere melting season. In this work, we performed two case studies over the Greenland Ice Sheet to quantify volumetric scattering in ICESat-2 signals over snow. Elevation data from ICESat-2 was compared to Airborne Topographic Mapper (ATM) data to quantify bias. We used snow optical grain sizes derived from ATM and the Next Generation Airborne Visible/Infrared Imaging Spectrometer (AVIRIS-NG) to attribute altimetry bias to snowpack properties. For the first case study, the mean optical grain sizes were 340±65 μm (AVIRIS-NG) and 670±420 μm (ATM), which corresponded with a mean altimetry bias of 4.81±1.76 cm in ATM. We observed larger grain sizes for the second case study, with a mean grain size of 910±381 μm and biases of 6.42±1.77 cm (ICESat-2) and 9.82±0.97 cm (ATM). Although these altimetry biases are within the accuracy requirements of the ICESat-2 mission, we cannot rule out more significant errors over coarse-grained snow, particularly during the Northern Hemisphere melting season.

Plain Language Summary

The Ice, Cloud, and Land Elevation Satellite-2 (ICESat-2) mission has been used to measure changes in land ice, vegetation cover, and sea ice, and there is growing interest to use ICESat-2 for snow science. ICESat-2 uses a lidar that operates at a green wavelength, through which it estimates the elevation of Earth's surface based on the time it takes for the laser to travel between the satellite and the surface. Snow weakly absorbs green light and can increase the travel time of the laser, which would introduce errors in elevation measurements. In this study, we used ICESat-2 and airborne lidar and spectrometer data to (i) identify errors in the ICESat-2 data and (ii) link the errors to snow properties over the Greenland Ice Sheet. We found that ICESat-2 errors have a link with snow grain size and density. The errors are within the accuracy requirements of ICESat-2, but more significant errors may be possible during the Northern Hemisphere melting season.

1 Introduction

The Ice, Cloud, and Land Elevation Satellite-2 (ICESat-2) was launched in September 2018 to perform measurements of surface height over glaciers and ice sheets (Markus et al., 2017). Since then, ICESat-2 data products have been developed to estimate the surface height of land ice, vegetation canopies, and sea ice (Smith et al., 2019; Kwok et al., 2019; Neuenschwander & Pitts, 2019). The sole onboard instrument, the Advanced Topographic Laser Altimeter System (ATLAS), emits laser light at 532 nm and produces high spatial resolution data (12 m footprint diameter and 10 kHz pulse repetition frequency) and a required accuracy of 0.4 cm yr^{-1} for ice sheet annual elevation change (Markus et al., 2017). Recent comparisons with ground-based data have shown that the ATLAS laser has a measured accuracy of <4 cm over ice sheet interiors (Brunt et al., 2021).

There is growing interest in the snow science community to use ICESat-2 to derive snow depth over remote locations through comparison of snow-on and snow-off elevations. A complication with past snow studies is that forested and mountainous environments have significant seasonal snow, yet these regions are subject to elevation uncertainty in ground-based and airborne surveys. In recent years, digital elevation models (DEMs) from lidar have become common data sets for snow depth estimates (Deems et al., 2013), though current lidar acquisitions are limited to airborne and ground-based

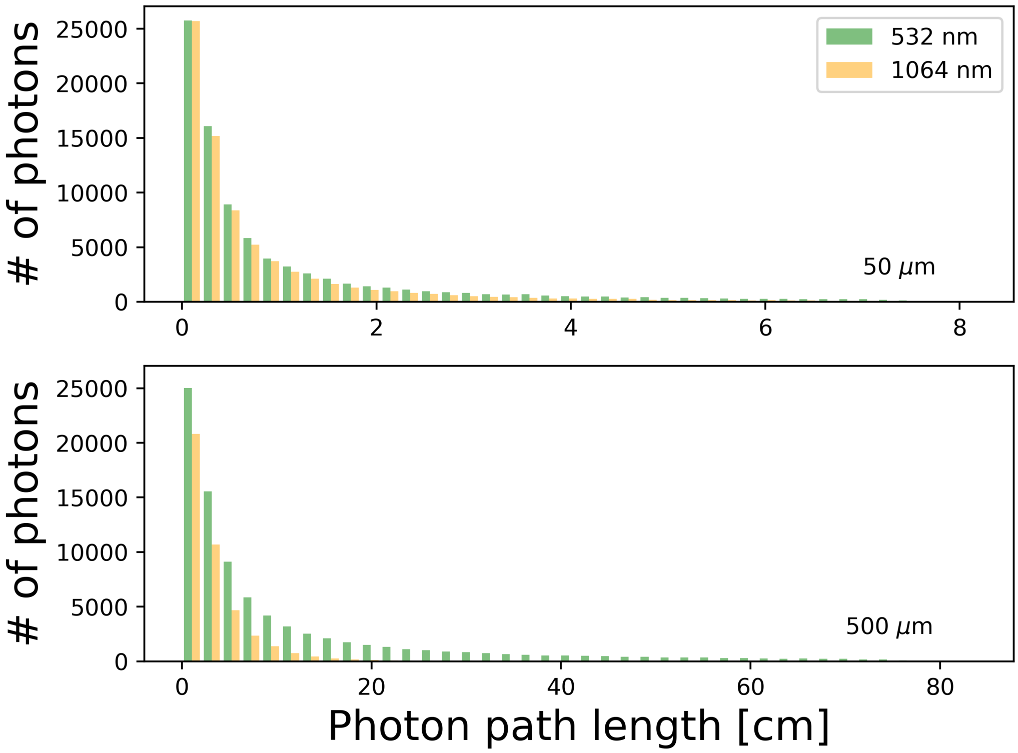

Figure 1. Histograms of 100000 photon path lengths traveled through a simulated, semi-infinite snowpack. The snow is assumed to be clean (i.e., no impurities) with ρ_s=400 kg m^{-3} and r_{eff}=50 μm (top), r_{eff}=500 μm (bottom). The range of path lengths differs between histograms to highlight the effects of volumetric scattering.

surveys. There are currently no documented efforts to measure deep snow in forests and mountains using spaceborne instrumentation (Bormann et al., 2018), so ICESat-2 has the potential to support snow studies through inter-seasonal measurements of terrain height.

A possible complication is that a laser shot from ICESat-2 may experience multiple scattering events within a snow layer before returning to the detector (Perovich, 2007) due to weak absorption of visible light (Warren & Wiscombe, 1980). This phenomenon, which we refer to as "volumetric scattering", is greatest in clean, coarse-grained snow, where the increased path length between individual snow particles will introduce a delay time in the returned laser pulse. The optical grain size of snow, a quantity used to represent snow grains as simplified shapes, is strongly linked to photon path length. Figure 1 shows the modeled effects of volumetric scattering by spherical snow particles at common lidar wavelengths. The path length traveled by photons within a snowpack is similar between 532 nm and 1064 nm at small optical grain sizes, but the path lengths at 532 nm increase with grain size. Near-infrared snow reflectance is low in snow with an optical grain size of 500 μm, so fewer 1064 nm photons propagate through the snowpack. Snow impurities may attenuate the ICESat-2 signal and reduce volumetric scattering bias, though impurity content has significant variability at small spatial and temporal scales (Flanner et al., 2007; Skiles et al., 2017).

Previous studies have assessed the potential impacts of snow on lidar measurements at 532 nm. Harding et al. (2011) found that return waveforms from an airborne 532 nm lidar experienced significant pulse broadening over snow, resulting in range biases on the

Table 1. Data Summary

Instrument	Dataset	Wavelengths	Case Study	Application
ICESat-2	ATL03	532 nm	$CS2$	Altimetry
ATM	ILNSAW1B ILNIRW1B	532 nm 1064 nm	$CS1$, $CS2$	Altimetry, Snow grain size
AVIRIS-NG	L2 Reflectance	380-2510 nm	$CS1$	Snow grain size

order of a few centimeters. A modeling study by Kerekes et al. (2012) found that centimeter-level biases occurred most frequently when the optical grain size of snow was 500 μm or more, and the amplitude of received waveforms was low relative to fine-grained snow returns. Smith et al. (2018) simulated ICESat-2 measurements over a snow-covered surface using a suite of surface height estimation techniques. The authors concluded that elevation biases may exceed 0.45 m over regions of clean, coarse-grained snow if the current ICESat-2 height estimation scheme is used for retrieved photons, though biases could decrease if other techniques are used or if snow impurities (i.e., black carbon) are present.

At the time of writing, the ICESat-2 mission has collected over 3 years of altimetry measurements over high-latitude regions, yet there have been no documented efforts to quantify volumetric scattering biases over snow. As part of an extensive validation effort, Operation IceBridge (OIB) launched a series of flights over Greenland late in the 2019 melt season. The flights collected elevation measurements using the Airborne Topographic Mapper (ATM), a lidar that operated at 532 nm and 1064 nm during the 2019 flights. Near-coincident flights were performed with the Next Generation Airborne Visible/Infrared Imaging Spectrometer (AVIRIS-NG) to retrieve hyperspectral reflectance and the optical grain size of snow.

Here we perform two case studies to assess bias in ICESat-2 and ATM altimetry measurements due to volumetric scattering in snow. Optical grain sizes derived from AVIRIS-NG reflectance data and ATM waveforms serve as input to a Monte Carlo ray tracing model to simulate altimetry bias over the Greenland ablation zone. In parallel, surface heights derived from ICESat-2 and the ATM 532 nm beam are compared to the ATM 1064 nm beam, which we assume also measures the surface, to estimate observed bias. The findings presented here will serve as a benchmark for an ICESat-2 bias correction algorithm over snow-covered surfaces.

2 Data Description and Case Study Locations

2.1 Case Study Locations

We performed two case studies over the Greenland ablation zone, which we refer to as $CS1$ and $CS2$ in the remainder of the paper. The locations of the study regions are shown in Figure 2, and Table 1 outlines the data sets used for each.

The first case study ($CS1$), performed for September 6, 2019, is located at coordinates 75.316-75.438°N, 56.528-56.778°W. This date and location correspond with a significant overlap between ATM and AVIRIS-NG flights, with ∼40 km of OIB flight data overlapping with AVIRIS-NG surveys. The ice surface features many crevasses and refreezing supraglacial lakes during this time of year, several of which were observed by ATM and AVIRIS-NG. The lakes are characterized by anomalously high optical grain

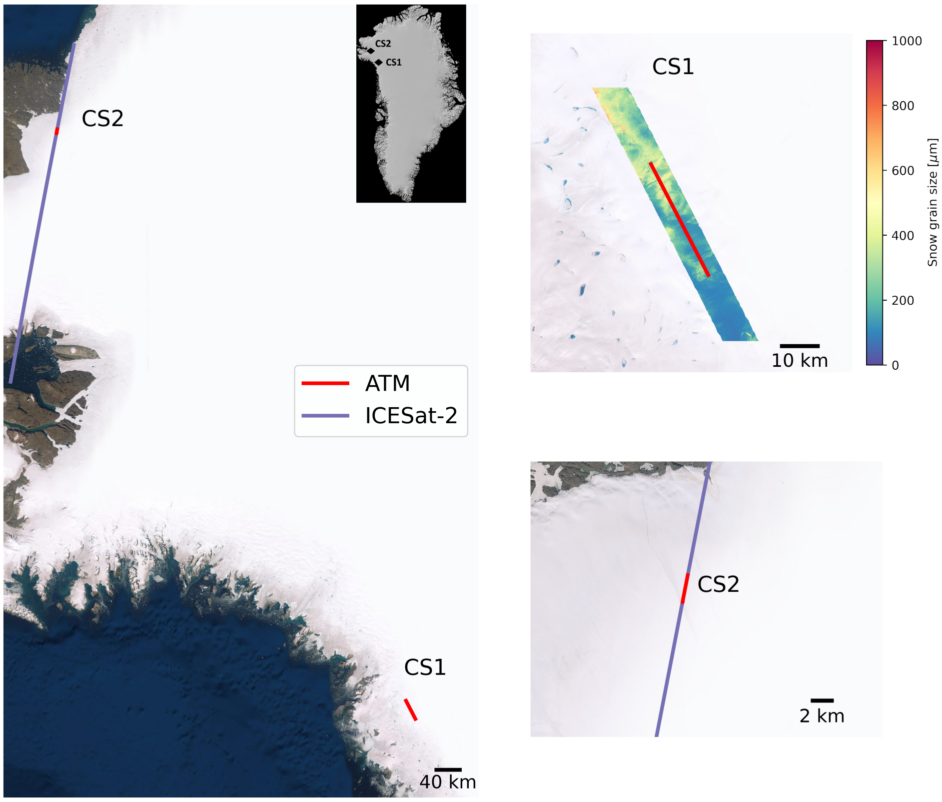

Figure 2. Landsat-8 imagery showing the location of the two case studies over the Greenland Ice Sheet. The red line given for CS1 (top right) is the path flown by both ATM and AVIRIS-NG, and the false color overlay is the snow grain sizes observed by AVIRIS-NG. The red line shown for CS2 (bottom right) represents the region where ATM and the central strong ground track of ICESat-2 (GT2L) intersect.

sizes in the AVIRIS-NG data, whereas the ATM beams exhibit a greater degree of noise over crevassed ice. These features are small relative to the size of the instrument swaths, so we applied a moving mean filter with a window size of 500 samples (30 m) to mitigate noise. There were no significant overlaps with ICESat-2 data over this region, so we used $CS1$ as a proof-of-concept to demonstrate green light penetration in snow.

The second case study ($CS2$) was performed for September 4, 2019 at coordinates 78.783-78.807°N, 66.066-66.090°W. Across this region, ATM followed an ICESat-2 overpass for 20 minutes, closely matching with the central ICESat-2 ground tracks (GT2L/GT2R). The ATM products used in this study (Section 2.2.1) have a swath width smaller than the distance between GT2L and GT2R, so the aircraft overlapped the two beams in alternating segments. Local topography can have a first-order impact on our analysis (Wang et al., 2019), where ∼10 m of separation between ATM and an ICESat-2 beam may lead to significant differences in elevation estimates, particularly over rough terrain. We therefore limited our analysis to regions where ATM footprints were within the ICESat-2 footprint, or a maximum distance of 12 m (Magruder et al., 2021). This restriction minimized errors due to data separation, but it also limited the analysis to a 2.5 km region over the ice sheet interior ($CS2$ in Figure 2, green line).

2.2 Altimetry Data

2.2.1 ATM

ATM is an altimetric lidar that has been used for high-latitude elevation measurements since 1993 (Brock et al., 2002; Krabill et al., 2002). In recent years, it has been used to validate ICESat-2 surface height estimates over sea ice and the 88°S transect of Antarctica (Kwok et al., 2020; Brunt et al., 2021) as part of Operation IceBridge. The instrument suite is composed of two laser altimeters that feature off-nadir scan angles 2.5° and 15°, which correspond to swath widths of 40 m and 245 m at typical flight altitudes. The 2.5° "narrow swath" altimeter is a dual-color laser that operates at 532 nm (green) and 1064 nm (near-infrared) simultaneously. The near-infrared laser has a footprint diameter of 0.91 m, or 40% larger than the 532 nm beam (0.64 m).

Here, we used two Level-1B Narrow-Swath data products: the Elevation and Return Strength with Waveforms (ILNSAW1B) and the Near-Infrared Waveforms (ILNIR1B). Both data products include information about the transmitted and received waveforms, including the amplitude and width of each waveform and the corresponding aircraft-surface range estimates. The ranges are derived using the centroid (median) time of the transmitted and received pulses, and these ranges are compared to the WGS84 ellipsoid to estimate surface elevation (Brock et al., 2002). Brunt, Neumann, and Larsen (2019) found that the 532 nm laser agrees well with ground-based measurements over the 88°S transect of Antarctica, with a mean uncertainty of ∼8.5 cm.

2.2.2 ICESat-2

ICESat-2 is a polar orbiting satellite with an operational altitude of 500 km and a 91-day repeat cycle. A single ATLAS 532 nm laser pulse is split into six beams that are configured in pairs, with a 90 m separation between beams within a pair and a 3.3 km separation between pairs (Neumann et al., 2019). The beams are named according to their ground track from left to right: GT1L/R, GT2L/R, and GT3L/R. At its operational altitude, ICESat-2 has a surface footprint of 12 m, which allows for significant overlap with its 0.7 m along-track resolution.

The ATLAS product used here is the ATL03 Global Geolocated Photon Data V005 (Neumann et al., 2020), which consists of latitude, longitude, and surface elevation for received photons. Each tagged photon is also classified as either signal or solar background, based on a statistical confidence algorithm (Neumann et al., 2019). Although noisier than other ICESat-2 data sets, we selected ATL03 to better capture the scattering experienced by individual photons. The number of photon returns was high over the Greenland Ice Sheet, so we only considered high confidence photons. The OIB flights over $CS2$ overlapped with the central beams in alternating segments. We selected a 2 km extent where OIB flew inline with the central strong beam (Figure 2, bottom right) to ensure that we received a high rate of photons across the study area. Comparisons with ground-based measurements over the 88°S transect show a mean uncertainty of ∼4 cm for ATL03 (Brunt et al., 2021).

We briefly consider the impacts of volumetric scattering on ATL06, the Land Ice Height Product V005 (Smith et al., 2019). The ATL06 algorithm aggregates geolocated ATL03 photons into 40 m segments, from which a mean surface height is derived. ATL06 segment values are posted every 20 m, yielding a 50% overlap between consecutive segments. Brunt, Neumann, and Smith (2019) found that ATL03 photon-based heights are generally a few centimeters higher than those from ATL06 segments due to differences in the processing algorithms. We only consider high-confidence ATL03 photons with ATM data in close proximity, so additional errors relative to ATL06 (which considers photons of low, medium, and high confidence and corrects for several instrument effects) are expected.

2.3 Snow Grain Size Data

2.3.1 AVIRIS-NG

The Next Generation Airborne Visible/Infrared Imaging Spectrometer is an airborne hyperspectral imager that has been used to retrieve surface radiances since 1986 (Gao et al., 1993; Green et al., 1998). Originally operating at 10 nm spectral resolution, the instrument now observes the Earth's surface between 380 and 2510 nm at a spectral resolution of 5 nm. Surface reflectances are derived from the radiances by applying an atmospheric correction and orthorectification. Reflectances from AVIRIS-NG generally have an accuracy within 2-5% (Thompson et al., 2019). The spectrometer has been used for a suite of applications since its inception, including vegetation mapping, trace gas identification, and retrieval of snow grain size (Kokaly et al., 2003; Thorpe et al., 2016; Nolin & Dozier, 2000).

We used AVIRIS-NG reflectances for $CS1$ to derive the optical grain size of snow for comparison against the altimetry data. An inversion algorithm derived by (Nolin & Dozier, 2000) was used to relate changes in the ice absorption feature at 1.03 μm to changes in optical grain size. In short, the algorithm compares AVIRIS-NG reflectances to those derived from a radiative transfer model to show that optical grain size increases as the near-infrared snow reflectance decreases. The snow is assumed to be composed of spherical ice particles, and snow impurities are assumed to have a negligible impact on the retrievals. Although impurity content is assumed to be negligible over the regions of interest, we recognize that impurities such as ice algae or cryoconite may impact retrievals over the Greenland ablation zone (Cook et al., 2020). Optical grain sizes derived from this algorithm have a stated uncertainty of 50 μm (Nolin & Dozier, 2000; Fair et al., 2022).

2.3.2 ATM

AVIRIS-NG grain sizes were unavailable over $CS2$, so we instead used an algorithm that infers grain size from ATM data. Over snow, subsurface scattering affects green ATM waveforms by reducing the maximum amplitude and increasing the width of the received pulse (Smith et al., 2018). The algorithm exploits this occurrence to compare waveforms from the ILNSAW1B product (Section 2.2.1) to an idealized waveform with no subsurface scattering. The grain size is then estimated based on differences in amplitude and pulse width. The model waveform is derived assuming that the snow has no impurities and has a density of 400 kg m^{-3}. While the former assumption is reasonable over this region of the Greenland Ice Sheet (Flanner et al., 2007), the assumed snow density is higher than typical values (Fausto et al., 2018; Schaller et al., 2016). The algorithm is also more sensitive to subsurface snow properties, so grain sizes derived by ATM are generally higher than those found using AVIRIS-NG (Section 4).

3 Methods

3.1 Monte Carlo Modeling

We first estimated altimetry bias using a combination of optical grain size data and Monte Carlo modeling. The model fires photons into a simulated semi-infinite snowpack and records their total path length until they are absorbed or leave the medium (Schneider et al., 2019). The snowpack has user-prescribed optical grain sizes and density, and it is configured to have spherical ice particles with negligible impurity content. The model has additional inputs for solar zenith and particle surface roughness, but we assumed that (i) the snow particles were smooth and (ii) the solar zenith angle was equal to the mean solar geometry observed at the time of flight for ATM. The snowpack was also assumed to have a uniform optical grain size.

The Monte Carlo model was used to benchmark lidar delay time within a snowpack. Simulations were conducted for different permutations of photon wavelength, snow density, and optical grain size. The simulations launched 10^5 photons into a snowpack at wavelengths 532 nm and 1064 nm to emulate the ATM dual-colored laser interacting with a snow-covered surface. We performed these simulations for grain sizes 50-1500 μm at 50 μm resolution. We then applied spline curve fitting to improve the resolution to 1 μm. Snow density was configured to be consistent with observations by Fausto et al. (2018), i.e. 315 kg m^{-3}. We obtained the path length traveled by the photons that escaped from the top of the snowpack, and for each wavelength the median path length of escaped photons was calculated to replicate the reference photon technique employed by ICESat-2 (Neumann et al., 2020). The median path length was treated as the surface height offset relative to an unbiased measurement. If we treat the 532 nm path lengths as biased surface height measurements (L_{532}) and the 1064 nm path lengths as ideal measurements (L_{1064}), then the modeled bias estimate ΔL is simply:

$$\Delta L = L_{532} - L_{1064} \tag{1}$$

In this configuration, a positive ΔL implies that 532 nm photons traveled a greater distance within the snowpack, which would suggest a negative bias in the final surface height estimate. Conversely, the 1064 nm path length (surface height) will be biased high (low) if there is a negative ΔL. Modeled biases were placed into lookup tables depending on the density used in the simulation. The result was six lookup tables that each had 1500 bias estimates as a function of optical grain size, given $\rho_s = [100, 200, 300, 315, 400, 500]$ kg m^{-3}. The biases in these lookup tables are the errors we would expect if grain size were the only factor impacting ICESat-2 and ATM observations.

3.2 Observed Bias

We look for bias in the altimetry data by comparing 532 nm elevation estimates with those from the ATM 1064 nm beam. The ATM beams periodically did not record laser pulses, so we applied a co-registration algorithm to match data samples from both beams. Because the beams fire simultaneously, the algorithm co-registers shots between beams by using the time stamps recorded for each laser pulse. The co-registered shots were then filtered to match with the central strong beam of ICESat-2 (see Section 2.3). For the first case study, rough terrain caused 17-21% signal loss in the ATM beams. Smoother ice was present for the second case study, so signal loss was lower (4-5%). Co-registered ICESat-2 and ATM elevations were used to approximate observed bias using Equation 1.

The accuracy of the ATM beams relative to each other has not been documented, so we performed a bias assessment of the two beams in the absence of snow. Operation IceBridge was flown from Qaanaaq Air Base (formerly Thule) in September 2019, and each flight included an overpass of the aircraft ramp for calibration purposes. We selected the ramp overpass from September 6 (Track 1730, Figure 4a), and Equation 1 was used to estimate bias over a dark, flat surface. Figure 4b shows the differences between the green and NIR beams. Comparisons over the ramp consistently feature negative bias, implying that NIR ranges surface heights are lower than those of the green beam. The bias has a nearly Gaussian distribution between -8 cm and 0 cm, with a slightly larger distribution toward less negative values (Figure 4c). Repeat flights over the ramp on different dates yielded similar results (Studinger, 2022). The median bias was -3.85 cm, and we applied this value as a correction factor to all comparisons between the ATM beams in the featured case studies.

To attribute altimetry bias to optical grain size, we co-registered ICESat-2 and corrected ATM laser pulses with AVIRIS-NG or ATM grain size estimates. We mapped each segment of grain size data with an estimate of modeled bias by matching grain sizes with the closest values found in each lookup table. In other words, each segment of co-registered data had six modeled bias estimates for each snowpack density given in Section 3.1. The observed biases were compared to matched model biases at these densities. If the observations agreed with at least one of the modeled results, then we could conclude that (i) the altimetry biases are linked to the optical grain size of snow and (ii) the bias is consistent with one of the given snow densities.

4 Results

4.1 Case Study 1

Model-derived results of altimetry bias have a strong dependence on snow optical grain size and density, as seen in Figure 3. At smaller grain sizes, bias is less sensitive to changes in snow density, particularly at grain sizes below 400 μm. Larger grain sizes exhibit greater dependence on snow density, especially when $\rho_s \leq 200$ kg m^{-3}. The largest modeled biases occur for $\rho_s = 100$ kg m^{-3}, up to a maximum of 37.84 cm at the largest grain sizes. At densities $\rho_s =$ 315-500 kg m^{-3} biases of 7.55-11.88 cm are more likely to occur. The bias asymptotically approaches zero with decreasing grain size at all densities, implying that little altimetry bias should be expected over fine-grained snow.

The AVIRIS-NG optical grain sizes co-registered with ATM are shown in Figure 5. The southern reaches of $CS1$ are characterized by grain sizes of $\leq$200 μm that typically increase near crevassed terrain or near melt ponds. In the northern portions of the flight track, grain sizes increase to 300-400 μm. This increase corresponds with a general decrease in surface elevation (Figure 6), with lower elevations implying warmer temperatures, greater melt, and faster snow metamorphism. Subsurface scattering on the order of 1-10 m is evident throughout the study area (green dots in Figure 6), indicating the presence of heavy crevassing. Although ATM waveform-fitted grain sizes exhibit similar trends to those from AVIRIS-NG, the derived values are much larger, with a mean grain size of 653$\pm$422 μm for ATM and 338$\pm$65 μm for AVIRIS-NG. ATM waveform-fitted grain sizes are derived as a function of received waveform amplitude and width, so we speculate in Section 5.2 that the estimated grain sizes are values obtained from subsurface snow.

Figure 7 shows that the small grain sizes at the start of $CS1$ correspond to negligible model bias and uncertainty due to snow density. In regions with larger grain sizes,

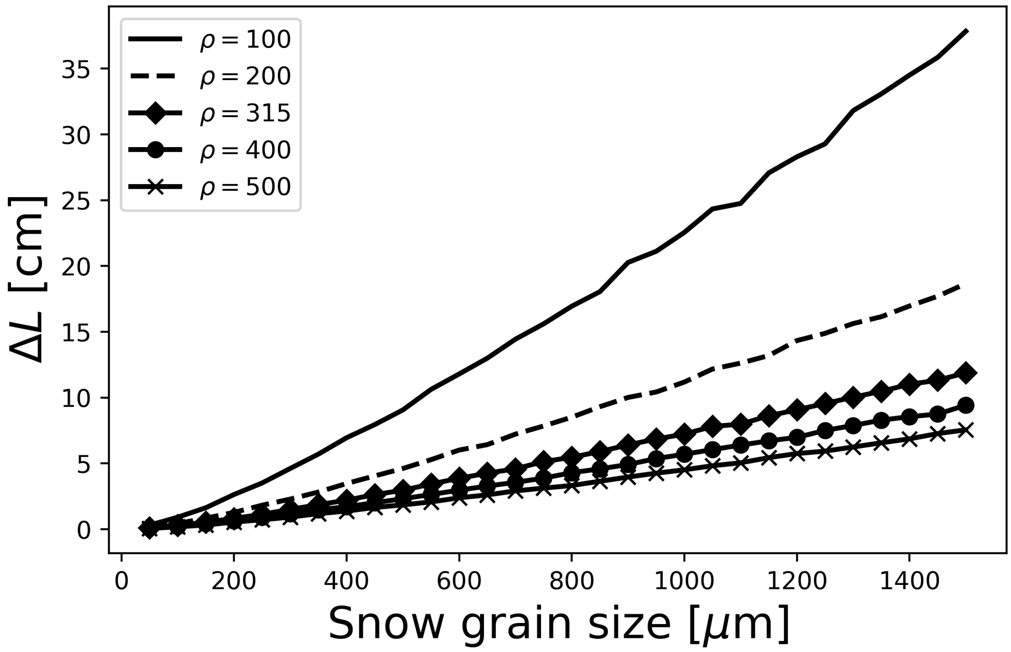

Figure 3. Modeled altimetry bias derived using median path lengths estimated from a Monte Carlo model (Schneider et al., 2019). Bias is given as a function of snow optical grain size and snowpack density. The snow density ρ_s = 315 kg m^{-3} is used to represent the average snow density reported over Greenland by Fausto et al. (2018) (ρ_s = 315 kg m^{-3}). The simulated bias at ρ_s = 300 kg m^{-3} is nearly identical to that of ρ_s = 315 kg m^{-3} and was thus omitted.

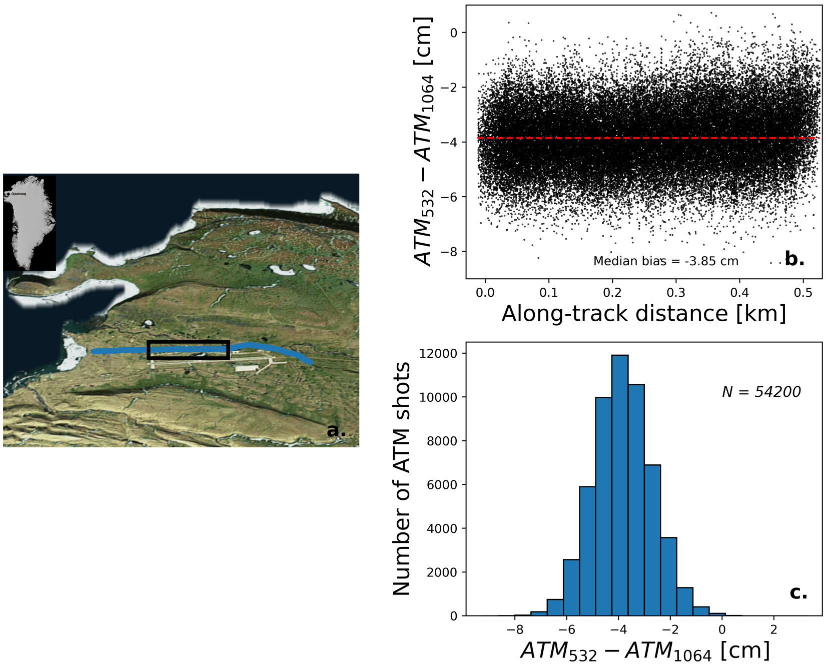

Figure 4. (a) Location of the aircraft ramp used to assess the bias between the ATM 532 nm and 1064 nm beams. The black box highlights the ramp overpass. (b) Along-track scatter plot of the 532 nm bias relative to 1064 nm measurements. Negative values indicate lower surface heights measured by the 1064 nm beam. The red dashed line depicts the median bias observed across the overpass. (c) Bias distribution between the ATM beams, as derived from ramp overpass measurements.

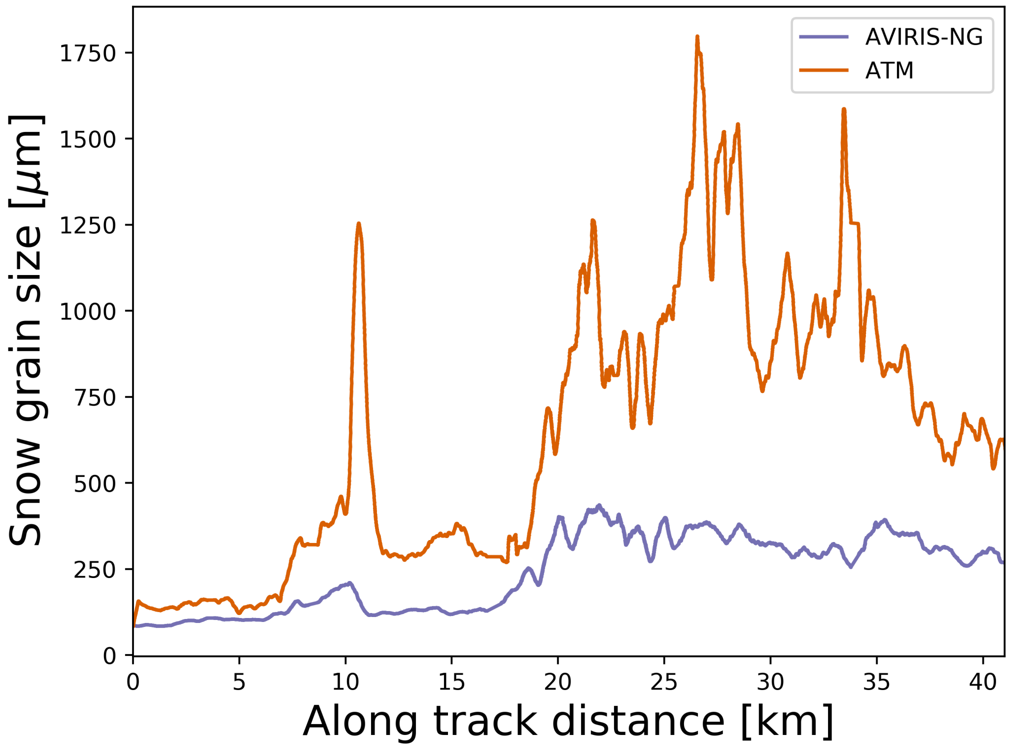

Figure 5. Snow optical grain sizes derived along-track from AVIRIS-NG (purple) and ATM waveforms (orange) for CS1.

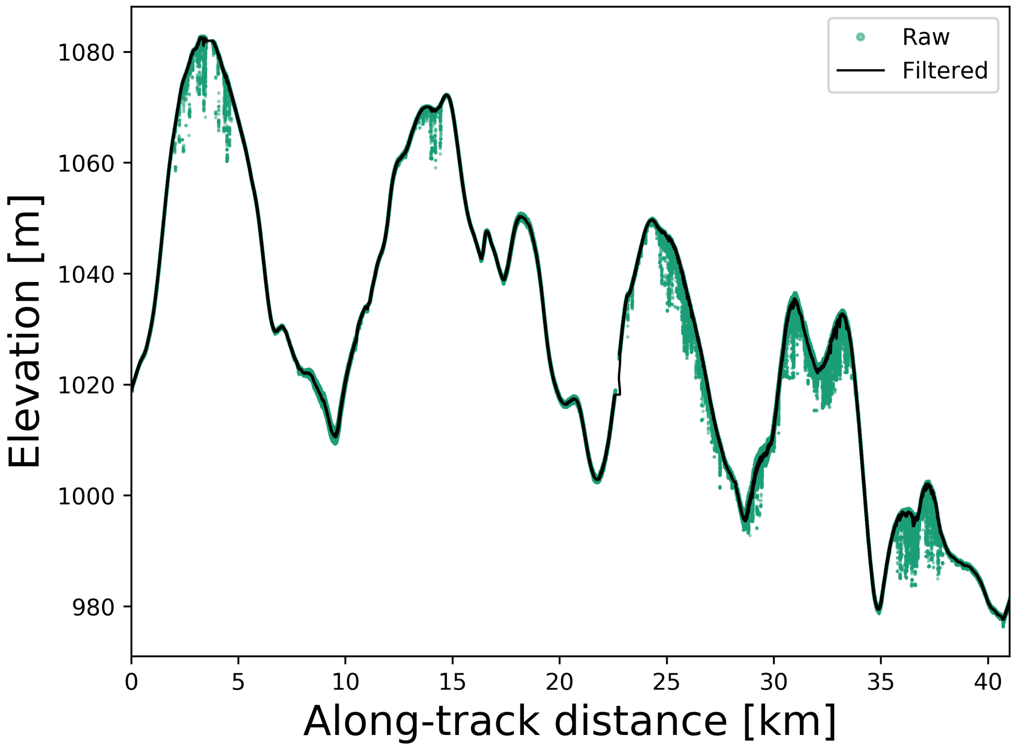

Figure 6. Surface heights for $CS1$, as given by ILNSAWL1B ("Raw", green dots). A moving mean filter (black line) was applied to remove features significantly below the surface.

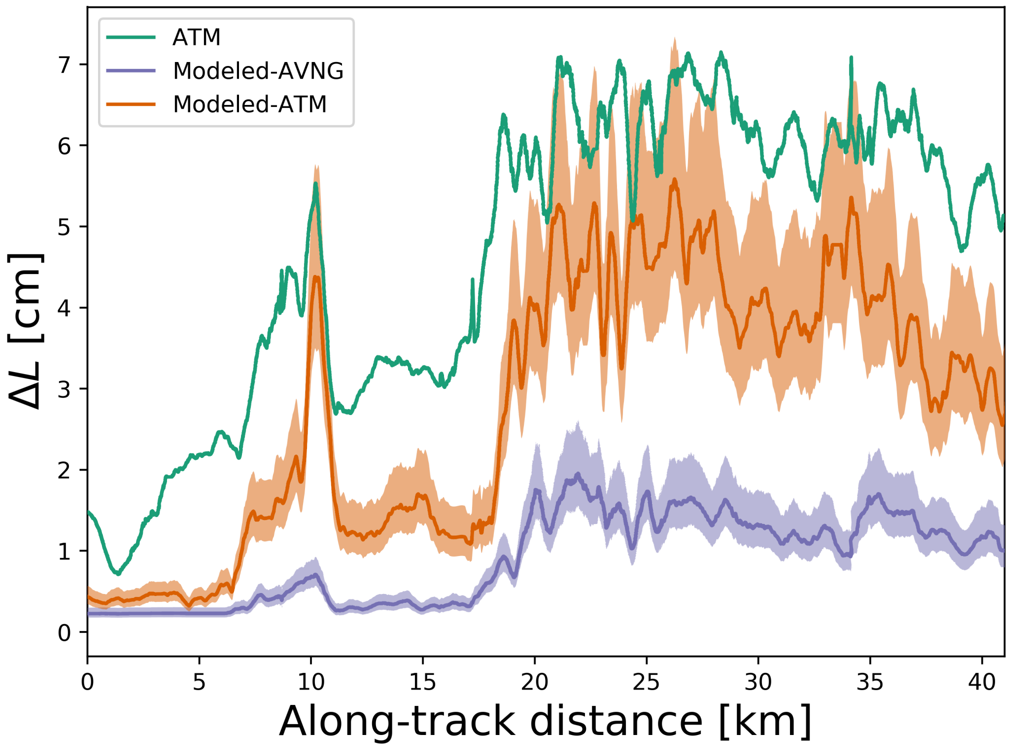

Figure 7. Observed ATM green-NIR range differences (green) as compared to modeled estimates using optical grain sizes from AVIRIS-NG reflectances (purple) and ATM waveform fitting (orange). The solid lines for the modeled estimates represents ρ_s = 400 kg m^{-3}, whereas the shading is the uncertainty to due changes in snow density, given ρ_s = 315-500 kg m^{-3}.

the bias increases, with the full extent dependent on the optical grain sizes used as model input. The lower grain sizes of AVIRIS-NG correspond with a maximum bias of 1.95±0.39 cm, whereas bias peaks at 5.58±1.12 cm with ATM waveform-fitted grain sizes. The green-NIR path length differences generally show agreement with the model when the ATM grain size algorithm is used, with the ATM-derived model estimates accounting for 71% of the observed bias. The best agreement between the model and the observations is in regions of larger optical grain size. The model underestimates bias relative to the observations at smaller grain sizes, suggesting that (a) the observations may agree better with snow densities of ρ_s = 200-250 kg m^{-3}, or (b) other factors are influencing the bias in this region.

4.2 Case Study 2

The optical grain sizes and along-track surface heights for $CS2$ are given in Figures 8 and 9. The region features gently sloped terrain that decreases in surface height over the track. At the large scale, co-registered ATM 532 nm and ICESat-2 data show general agreement in surface height trends. The ICESat-2 data has slighly larger variability among individual photons which may be attributed to the inherent noisiness of the ATL03 product. The mean bias between the ATM 532 nm heights and ICESat-2 heights is ∼1 cm, with a precision of 10 cm. The grain sizes are comparable to those derived over $CS1$, with a mean value of 910±381 μm. The variability in grain size is larger than in $CS1$, though this is likely due to the smaller spatial scale. A surface feature at 1.3 km

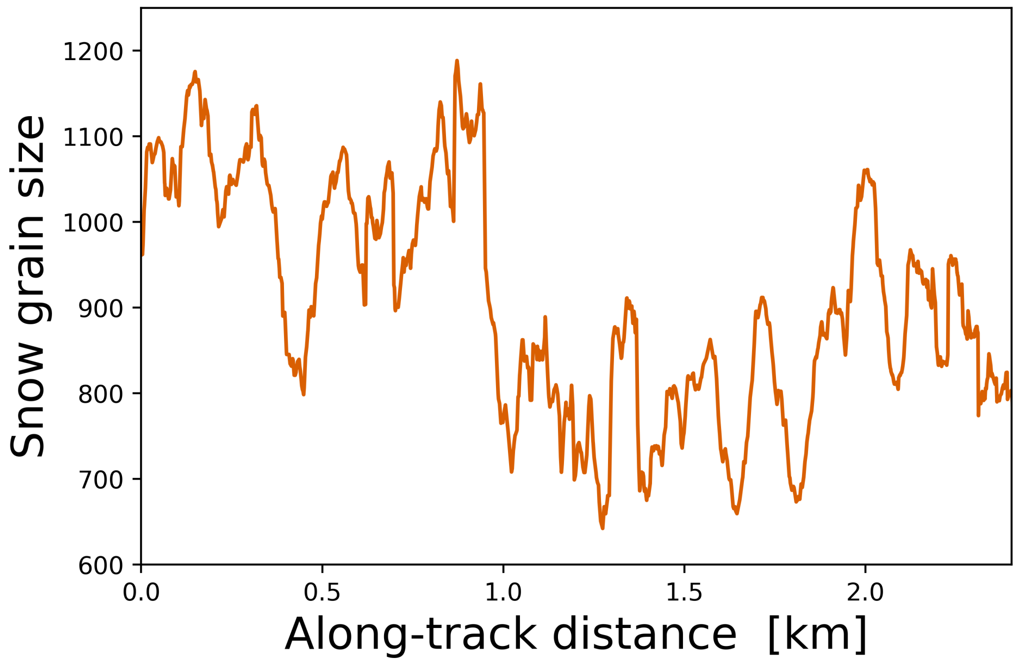

Figure 8. Snow optical grain sizes for CS2, as derived from 532 nm ATM waveforms.

along-track corresponds with a localized increase in grain size and greater disagreement between the altimeters. The ICESat-2 observations have a greater spread at this feature that is not replicated in ATM, suggesting the presence of a shallow melt pond or crevasse that was undetected by ATM pulses co-registered with ICESat-2.

Despite the variability in optical grain size, the modeled bias over $CS2$ peaks at 6.7 cm at the start of the track before decreasing to ∼5.5 cm as grain size decreases. The mean modeled bias across the region is 4.93±1.89 cm. Between the two altimeters, ICESat-2 bias trends show the closest agreement to modeled estimates. The ICESat-2 biases peak at 17.64 cm at the start of the track before reducing to 6.42±1.77 cm. The ATM green-NIR range differences show weaker agreement with the model than in $CS1$, with a mean bias of 9.82±0.97 cm. However, ATM trends resemble those seen in the model, implying that optical grain size still has an influence on ATM signals. Overall, the model accounts for 66% (ATM) and 95% (ICESat-2) of the observed bias. The rough surface feature at 1.3 km produces the greatest disagreement between the altimeters and the model, with ICESat-2 showing the greatest agreement with the 1064 nm beam and ATM 532 nm having the weakest. We speculate that ATM 532 nm and ICESat-2 illuminated different components of the surface feature, as the model results suggest that optical grain size contributed little to the biases over this region.

5 Discussion

5.1 Modeled and Observed Bias

The relationship between optical grain size and ICESat-2 bias is a function of the path length of signal photons incident upon a snow surface. When photons interact with snow, there are two potential outcomes: reflection after subsurface scattering or absorption by the snowpack. The first outcome is more frequent for ICESat-2 and the ATM 532 nm beam over coarse-grained snow, and it is responsible for the largest biases over

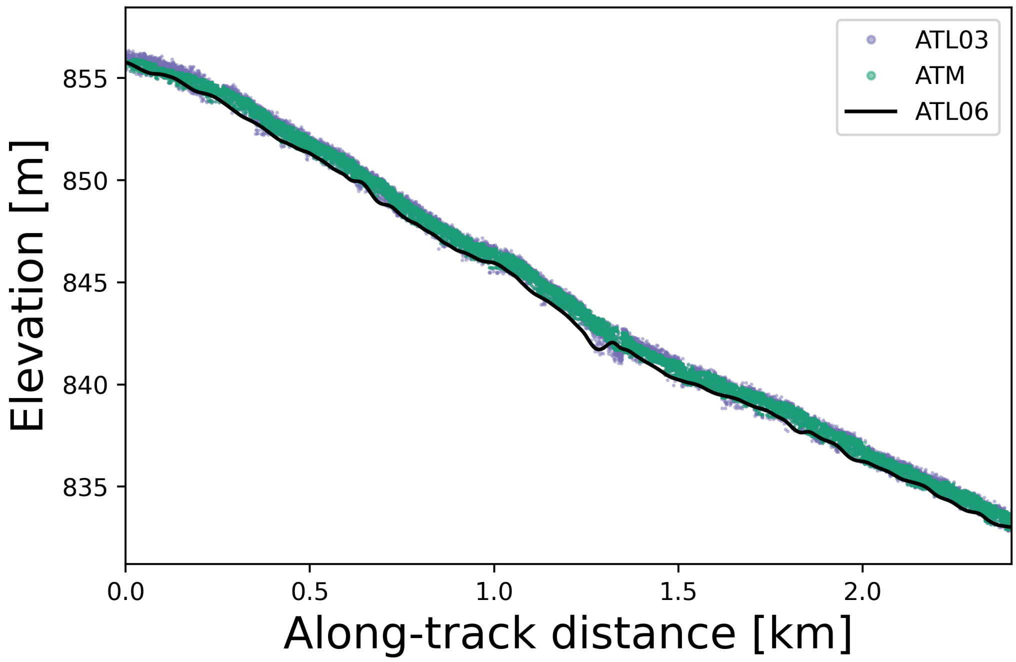

Figure 9. Along-track surface heights from ATL03 (light blue), the ATM 532 nm beam (green), and ATL06 (black). The plot only includes spot measurements where ATM was within 12 m of ICESat-2 footprints.

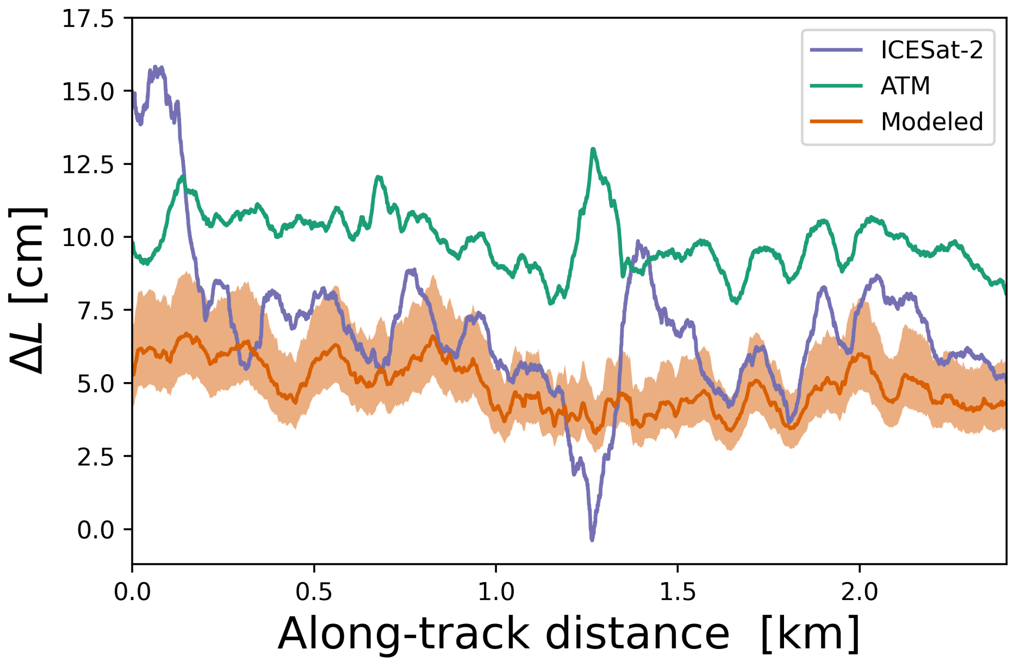

Figure 10. Observed ICESat-2 (purple) and ATM (green) elevation bias, compared to modeled biases using ATM grain sizes at ρ_s = 315-500 kg m^{-3} (orange).

the Greenland Ice Sheet. The second outcome occurs with the ATM 1064 nm beam when grain size is large, due to the low reflectance of aged snow in this part of the electromagnetic spectrum. Snow absorption reduces the occurrence of multiple scattering in NIR signals, so bias will be low over snow surfaces. The presence of snow impurities, such as black carbon and ice algae, may increase the probability of absorption for 532 nm signals and reduce bias (Smith et al., 2018), but further research is needed to confirm this hypothesis.

Model-derived results of altimetry bias have a strong dependence on optical grain size and density. As seen in Figure 3, the dependence on snow density is minor at small grain sizes, particularly at snow densities expected over Greenland. The modeled bias asymptotically approaches zero when grain size is small, which implies that the bias between two altimeters should be negligible when excluding other factors. Although discrepancies in bias become more evident between snow densities at larger grain sizes, we note that lower densities (i.e., ρ_s = 100-200 kg m^{-3}) only occur for fresh snow. The case studies presented here take place at the end of the Greenland melt season, where snow densities of ρ_s = 300-500 kg m^{-3} and larger grain sizes are more common, as supported by the observations of Schaller et al. (2016) and Fausto et al. (2018).

5.2 Sources of Uncertainty

In $CS1$, we found that optical grain size retrievals differed substantially in magnitude between AVIRIS-NG and ATM. The exact cause may be related to the respective retrieval methods. Grain sizes from AVIRIS-NG are derived from the near-infrared surface reflectance of a location, so they are more sensitive to changes in surface snow properties. The ATM algorithm estimates grain size through received waveform pulses, which contain backscatter from below the snow surface if volumetric scattering is significant. The differences between the two algorithms are evident in Figure 5, which can be separated into fine-grained and coarse-grained regions, which correspond to sections 0-17 km and 17-42 km along the $CS1$ transect, respectively. In the fine-grained region, the pore spacing between snow grains is small, so ATM beam penetration beyond the surface layer will be minimal, and the derived optical grain size will be smaller as a consequence. Volumetric scattering becomes more significant at larger optical grain sizes, as is reflected in the coarse-grained region of Figure 5. If the surface grain sizes are large, then the ATM beam is more likely to penetrate the subsurface, where grain sizes may be larger than those observed by AVIRIS-NG at the surface. Although ICESat-2 was not considered in $CS1$, the strong agreement between ICESat-2 and modeled bias in Figure 10 indicates that retrieved ATL03 photon path lengths are more sensitive to subsurface grain sizes over aged or melting snow.

The data sets used here each have different approaches to estimating surface height, which may influence the biases given in Figures 7 and 10. Both ATM beams estimate surface height from the centroid of received waveforms, and a signal strength threshold is applied to filter noise. Although most background noise is removed with the threshold, sufficiently coarse snow or rough terrain may broaden waveforms and shift the centroid by nanoseconds, or centimeters in height change. ICESat-2 and the Monte Carlo model use similar approaches by estimating the median surface height (ICESat-2) or travel time (model) for photon aggregates. Subsurface scattering increases the distribution of photon delay times, therefore also increasing uncertainty and bias in ATL03 and the model. Thus, the differences between ATM and the model may be partly explained by these different approaches in signal processing. The two bias estimates show better agreement in the coarse-grained region of Figure 7, which may indicate that the model is neglecting snowpack features that impact the ATM signal. A model that allows for more complex scenarios, such as a rough surface layer or layer-dependent optical grain sizes, could help to answer these questions, though we leave the development of such a model to a future study.

As noted above, the ATL06 algorithm aggregates ATL03 photons, applies several corrections, and produces 40 m segment heights that are 3 cm lower than metrics based solely on ATL03 photon heights. Consequently, ATL06 biases in the presence of volumetric scattering should be 3 cm larger than the ATL03-based biases reported here. The impact of these biases should be greatest when comparing times of year with relatively little and relatively significant volumetric scattering, for example summer vs. winter surface heights. However, given the magnitude of seasonal elevation change in the ablation zone of Greenland, it may be difficult to isolate the magnitude of volumetric-scattering-based biases from the height change due to seasonal melt and accumulation.

5.3 Implications for Snow Studies

This study was performed to assess ICESat-2 measurements over snow. There has been increasing interest in using ICESat-2 to derive spaceborne measurements of snow depth (Bormann et al., 2018). Currently, digital elevation models from lidar are commonly used to estimate snow depth (Deems et al., 2013), though current lidar applications are restricted to airborne and ground-based surveys. There is a critical need to measure deep snow in forests and mountains using spaceborne instrumentation (Bormann et al., 2018; National Academies of Sciences, Engineering, and Medicine, 2018), and progress is this area is an objective of the NASA-sponsored Snow Experiment (SnowEx). ICESat-2 has the potential to support SnowEx objectives through interseasonal measurements of terrain height.

Field campaigns conducted for the SnowEx mission require measurements from the mid-latitude melting season, when the optical grain size of snow is largest. The results in Figure 10 indicate that ICESat-2 measurements over melting snow should be accurate to within $\sim$10 cm, assuming that the snow has compacted prior to melt. In contrast, ATM shows low bias for $CS1$, where the grain size is smaller. Although we were unable to consider ICESat-2 for $CS1$, the close agreement between ICESat-2 and ATM (Figure 10) implies that ICESat-2 would experience minimal bias over locations with fresh, fine-grained snow. Hence, utilizing ICESat-2 for accurate measurements of snow depth is possible, though melting or aged snow may introduce bias and uncertainty in uncorrected ATL03 measurements. Higher-level products, such as ATL06 or ATL08, may reduce noise from the ATL03 photon cloud, but they will retain biased snow surface heights if subsurface scattering is unaccounted for, particularly over shallow snow.

6 Conclusions

In this study, we used altimetry data from ICESat-2 and ATM to quantify volumetric scattering bias in snow. A fusion of airborne optical grain size retrievals and Monte Carlo modeling was used to predict altimetry bias over the western Greenland ablation zone at the end of the melt season. ICESat-2 and the green ATM beam were compared to the near-infrared ATM beam to estimate observed bias. Our results suggest a positive relationship between the optical grain size of snow and altimetry bias over two case studies. The modeled results show that snowpack density is an important driver for volumetric scattering, though actual biases in the study locations remained consistent with densities of $\sim$315-500 kg m^{-3}. Although bias in both altimeters was generally within 10 cm, we cannot rule out more significant biases near the peak of the Northern Hemisphere melting season, when snow grain coarsening will enhance volumetric scattering at all snow densities.

The results in $CS1$ indicate that retrieved snow grain size is dependent on the instrument used. Grain sizes from AVIRIS-NG appear to originate from the snow surface, whereas ATM retrieves larger grain sizes within the snow subsurface. When combined with the Monte Carlo model, both data sets adequately reproduce trends in volumetric scattering bias, though the magnitude of the observed bias is not fully captured. Although used here, both instruments have infrequent coverage over mid-latitude field sites, and ATM is not expected to collect data in the near future. Other sources of effective grain size, such as MODIS or Sentinel-3 (Painter et al., 2009; Mei et al., 2021), will therefore be needed for future volumetric scattering assessments over snow.

Further research is needed to identify altimetry biases in the presence of snowpack impurities or rough topography. The full impact of dust and black carbon on altimetry signals is not known, so there is a need for accurate airborne and satellite retrievals of surface impurity content. Similarly, a correction for rough or sloped terrain is needed, given that both factors increase height uncertainties for both ICESat-2 and ATM. To address these problems among others, a follow-up study is in preparation that validates the results in this paper over mid-latitude snow. The SnowEx mission is conducting airborne lidar surveys for its 2023 Alaska campaign, several of which are expected to have significant overlap with ICESat-2 tracks. The flights will overpass coastal and forested regions of Alaska, so we anticipate a more rigorous analysis of ICESat-2 over multiple terrain types. The expected result is a bias correction algorithm that ideally will be applicable to all snow surfaces.

7 Open Research

The ICESat-2 ATL03 data may be found at NSIDC (Neumann et al., 2021). The ATM 532 nm and 1064 nm data is provided by Studinger and Manizade (2020b) and Studinger and Manizade (2020a), respectively. The AVIRIS-NG optical grain size data was obtained through correspondence with John Chapman (john.w.chapman@jpl.nasa.gov) and Winston Olson-Duvall (winston.olson-duvall@jpl.nasa.gov). The AVIRIS-NG reflectances used to derive grain size may be obtained from Chapman and Olson-Duvall (2019).

Acknowledgments
This research was funded by NASA grant #80NSSC20K0062 and the NASA Postdoctoral Program (grant #NPP168273S). We are grateful to the ICESat-2 and Operation IceBridge teams for their insight on the two instruments. We also thank Michael Studinger for his guidance on how to quantify the bias between the ATM beams.

References

Bormann, K. J., Brown, R. D., Derksen, C., & Painter, T. H. (2018). Estimating snow-cover trends from space. *Nature Climate Change*, *8*, 924-928. doi: 10.1038/s41558-018-0318-3

Brock, J. C., Wright, C. W., Sallenger, A. H., Krabill, W. B., & Swift, R. N. (2002). Basis and methods of NASA Airborne Topographic Mapper lidar surveys for coastal studies. *Journal of Coastal Research*, *18*, 1-13.

Brunt, K., Neumann, T., & Larsen, C. (2019). Assessment of altimetry using ground-based GPS data from the 88S Traverse, Antarctica, in support of ICESat-2. *The Cryosphere*, *13*, 579–590. doi: 10.5194/tc-13-579-2019

Brunt, K., Neumann, T., & Smith, B. (2019). Assessment of ICESat-2 ice sheet surface heights, based on comparisons over the interior of the Antarctic Ice Sheet. *Geophysical Research Letters*, *46*, 13072–13078. doi: 10.1029/2019GL084886

Brunt, K., Smith, B., Sutterly, T., Kurtz, N., & Neumann, T. (2021). Comparisons of Satellite and Airborne Altimetry With Ground-Based Data From the Interior of the Antarctic Ice Sheet. *Geophysical Research Letters*, *48*. doi: 10.1029/2020GL090572

Chapman, J., & Olson-Duvall, W. (2019). *AVIRIS-NG L2 Orthocorrected and Atmospherically Corrected Reflectance.* Retrieved from `https://avirisng.jpl.nasa.gov/dataportal/`

Cook, J. M., Tedstone, A. J., Williamson, C., McCutcheon, J., Hodson, A. J., Dayal, A., … Tranter, M. (2020). Glacier algae accelerate melt rates on the south-western Greenland Ice Sheet. *The Cryosphere*, *14*, 309-330. doi: 10.5194/tc-14-309-2020

Deems, J. S., Painter, T. H., & Finnegan, D. C. (2013). Lidar measurement of snow depth: a review. *Journal of Glaciology*, *59*, 467-479. doi: 10.3189/2013JoG12J154

Fair, Z., Flanner, M., Schneider, A., & Skiles, S. M. (2022). Sensitivity of modeled snow grain size retrievals to solar geometry, snow particle asphericity, and snowpack impurities. *EGUsphere (preprint)*. doi: 10.5194/egusphere-2022-266

Fausto, R. S., Box, J. E., Vandecrux, B., van As, D., Steffen, K., MacFerrin, M. J., … Braithwaite, R. J. (2018). A snow density dataset for improving surface boundary conditions in Greenland Ice Sheet firn modeling. *Front. Earth Sci.*, *6*. doi: 10.3389/feart.2018.00051

Flanner, M. G., Zender, C. S., Randerson, J. T., & Rasch, P. J. (2007). Present-day climate forcing and response from black carbon in snow. *Journal of Geophysical Research Atmospheres*. doi: 10.1029/2006JD008003

Gao, B. C., Heidebrecht, K. B., & Goetz, A. F. (1993). Derivation of scaled surface reflectances from AVIRIS data. *Remote Sensing of Environment*. doi: 10.1016/0034-4257(93)90014-O

Green, R., Eastwood, C., Sarture, C. M., Chrien, T. G., Aronsson, M., Chippendale, B. J., … Williams, O. (1998). Imaging spectroscopy and the Airborne Visible/Infrared Imaging Spectrometer (AVIRIS). *Remote Sensing of Environment*, *65*, 227-248. doi: 10.1016/S0034-4257(98)00064-9

Harding, D., Dabney, P., Valett, S., Yu, A., Vasilyev, A., & Kelly, A. (2011). Airborne polarimetric, two-color laser altimeter measurements of lake ice cover: A pathfinder for NASA's ICESat-2 spaceflight mission. In *International geoscience and remote sensing symposium.* doi: 10.1109/IGARSS.2011.6050002

Kerekes, J., Goodenough, A., Brown, S., Zhang, J., Csatho, B., Schenk, A., … Wheelwright, R. (2012). First principles modeling for lidar sensing of complex ice surfaces. In *2012 ieee international geoscience and remote sensing symposium* (pp. 3241–3244). IEEE. doi: 10.1109/IGARSS.2012.6350733

Kokaly, R. F., Despain, D. G., Clark, R. N., & Livo, K. E. (2003). Mapping vegetation in Yellowstone National Park using spectral feature analysis of AVIRIS data. *Remote Sensing of Environment*, *83*, 437-456. doi: 10.1016/S0034-4257(02)00133-5

Krabill, W. B., Abdalati, W., Frederick, E. B., Manizade, S. S., Martin, C. F., Sonntag, J. G., … Yungel, J. G. (2002). Aircraft laser altimetry measurement of elevation changes of the Greenland Ice Sheet: technique and accuracy assessment. *Journal of Geodynamics*, *34*, 357–376. doi: 10.1016/S0264-3707(02)00040-6

Kwok, R., Kacimi, S., Markus, T., Kurtz, N. T., Studinger, M., Sonntag, J. G., … Harbeck, J. P. (2019). ICESat-2 surface height and sea ice freeboard assessed with ATM lidar acquisitions from Operation IceBridge. *Geophysical Research Letters*, *46*, 11228–11236. doi: 10.1029/2019GL084976

Kwok, R., Kacimi, S., Webster, M. A., Kurtz, N. T., & Petty, A. A. (2020). Arctic snow depth and sea ice thickness from ICESat-2 and CryoSat-2 freeboards: A first examination. *Journal of Geophysical Research: Oceans*. doi: 10.1029/2019JC016008

Magruder, L., Brunt, K., Neumann, T., Klotz, B., & Alonzo, M. (2021). Passive Ground-Based Optical Techniques for Monitoring the On-Orbit ICESat-2 Altimeter Geolocation and Footprint Diameter. *Earth and Space Science*, *8*. doi: 10.1029/2020EA001414

Markus, T., Neumann, T., Martino, A., Abdalati, W., Brunt, K., Csatho, B., … Zwally, J. (2017). The Ice, Cloud, and land Elevation Satellite-2 (ICESat-

2): Science requirements, concept, and implementation. *Remote Sensing of Environment*, *190*, 260–273. doi: 10.1016/j.rse.2016.12.029

Mei, L., Rozanov, V., Pohl, C., Vountas, M., & Burrows, J. P. (2021). The retrieval of snow properties from SLSTR Sentinel-3 – Part 1: Method description and sensitivity study. *The Cryosphere*, *15*, 2757-2780. doi: 10.5194/tc-15-2757-2021

National Academies of Sciences, Engineering, and Medicine. (2018). Thriving on our changing planet: A decadal strategy for earth observation from space. In (chap. 6). The National Academies Press. doi: https://doi.org/10.17226/24938

Neuenschwander, A., & Pitts, K. (2019). The ATL08 land and vegetation product for the ICESat-2 mission. *Remote Sensing of Environment*, *221*, 247-259. doi: 10.1016/j.rse.2018.11.005

Neumann, T., Brenner, A., Hancock, D., Robbins, J., Saba, J., Harbeck, J., ... Rebold, T. (2021). *ATLAS/ICESat-2 L2A Global Geolocated Photon Data, Version 5.* doi: 10.5067/ATLAS/ATL03.005

Neumann, T., Brenner, A., Hancock, D., Robbins, J., Saba, J., Harbeck, K., ... Rebold, T. (2020). *Ice, Clouds, and Land Elevation Satellite-2 (ICESat-2): Algorithm Theoretical Basis Document (ATBD) for Geolocated Photons* (Tech. Rep.). NASA Goddard Space Flight Center. Retrieved from `https://icesat-2.gsfc.nasa.gov/sites/default/files/u71/ICESat2_ATL03_ATBD_r003_v2.pdf`

Neumann, T., Martino, A. J., Markus, T., Bae, S., Bock, M. R., Brenner, A. C., ... Thomas, T. C. (2019). The Ice, Clouds and Land Elevation Satellite-2 mission: A global geolocated photon product derived from the Advanced Topographic Laser Altimeter System. *Remote Sensing of Environment*, *233*. doi: doi.org/10.1016/j.rse.2019.111325

Nolin, A. W., & Dozier, J. (2000). A hyperspectral method for remotely sensing the grain size of snow. *Remote Sensing of Environment*. doi: 10.1016/S0034-4257(00)00111-5

Painter, T. H., Rittger, K., McKenzie, C., Slaughter, P., Davis, R. E., & Dozier, J. (2009). Retrieval of subpixel snow covered area, grain size, and albedo from modis. *Remote Sensing of Environment*, *13*, 868-879. doi: https://doi.org/10.1016/j.rse.2009.01.001

Perovich, D. K. (2007). Light reflection and transmission by a temperate snow cover. *Journal of Glaciology*. doi: 10.3189/172756507782202919

Schaller, C. F., Freitag, J., Kipfstuhl, S., Laepple, T., Steen-Larsen, H. C., & Eisen, O. (2016). A representative density profile of the North Greenland snowpack. *The Cryosphere*, *10*, 1991-2002. doi: 10.5194/tc-10-1991-2016

Schneider, A., Flanner, M., De Roo, R., & Adolph, A. (2019). Monitoring of snow surface near-infrared bidirectional reflectance factors with added light-absorbing particles. *Cryosphere*. doi: 10.5194/tc-13-1753-2019

Skiles, S. M. K., Painter, T., & Okin, G. S. (2017). A method to retrieve the spectral complex refractive index and single scattering optical properties of dust deposited in mountain snow. *Journal of Glaciology*. doi: 10.1017/jog.2016.126

Smith, B., Fricker, H., Holschuh, N., Gardner, A. S., Adusumilli, S., Brunt, K., ... Siegfried, M. (2019). Land ice height-retrieval algorithm for NASA's ICESat-2 photon-counting laser altimeter. *Remote Sensing of Environment*, *233*. doi: 10.1016/j.rse.2019.111352

Smith, B., Gardner, A., Schneider, A., & Flanner, M. (2018). Modeling biases in laser-altimetry measurements caused by scattering of green light in snow. *Remote Sensing of Environment*, *215*, 398-410. doi: 10.1016/j.rse.2018.06.012

Studinger, M. (2022, Mar.). personal communication.

Studinger, M., & Manizade, S. (2020a). *IceBridge ATM L1B Near-Infrared Wave-*

forms, Version 1. doi: 10.5067/V25X7LHDPMZY

Studinger, M., & Manizade, S. (2020b). *IceBridge Narrow Swath ATM L1B Elevation and Return Strength with Waveforms, Version 1.* doi: 10.5067/V25X7LHDPMZY

Thompson, D. R., Guanter, L., Berk, A., Gao, B., Richter, R., Schäpfer, D., & Thome, K. J. (2019). Retrieval of atmospheric parameters and surface reflectance from visible and shortwave infrared imaging spectroscopy data. *Surveys in Geophysics*, *40*, 333-360. doi: 10.1007/s10712-018-9488-9

Thorpe, A. K., Frankenberg, C., Aubrey, A. D., Roberts, D. A., Nottrott, A. A., Rahn, T. A., ... McFadden, J. P. (2016). Mapping methane concentrations from a controlled release experiment using the next generation airborne visible/infrared imaging spectrometer (AVIRIS-NG). *Remote Sensing of Environment*, *179*, 104-115. doi: 10.1016/j.rse.2016.03.032

Wang, C., Zhu, C., Nie, S., Xi, X., Li, D., Zheng, W., & Chen, S. (2019). Ground elevation accuracy verification of ICESat-2 data: a case study in Alaska, USA. *Optics Express*, *27*. doi: 10.1364/OE.27.038168

Warren, S. G., & Wiscombe, W. J. (1980). A model for the spectral albedo of snow. II: snow containing atmospheric aerosols. *Journal of the Atmospheric Sciences*. doi: 10.1175/1520-0469(1980)037⟨2734:AMFTSA⟩2.0.CO;2